Geophys. J. Int. (2008) **174,** 1019–1028 doi: 10.1111/j.1365-246X.2008.03880.x

Seismic evidence for a sharp lithospheric base persisting to the lowermost mantle beneath the Caribbean

Tadashi Kito,[1,*] Christine Thomas,[1] Andreas Rietbrock,[1] Edward J. Garnero,[2] Stuart E. J. Nippress[1] and Andy E. Heath[1]

[1]*Department of Earth and Ocean Sciences, University of Liverpool, Liverpool, UK. E-mail: tadashi.kito@yale.edu*
[2]*School of Earth and Space Exploration, Arizona State University, Tempe, Arizona, USA*

Accepted 2008 June 9. Received 2008 April 2; in original form 2007 November 9

SUMMARY

Broad-band data from South American earthquakes recorded by Californian seismic networks are analysed using a newly developed seismic wave migration method—the slowness backazimuth weighted migration (SBWM). Using the SBWM, out-of-plane seismic *P*-wave reflections have been observed. The reflection locations extend throughout the Earth's lower mantle, down to the core–mantle boundary (CMB) and coincide with the edges of tomographically mapped high seismic velocities. Modelling using synthetic seismograms suggests that a narrow (10–15 km) low- or high-velocity lamella with about 2 per cent velocity contrast can reproduce the observed reflected waveforms, but other explanations may exist. Considering the reflection locations and synthetic modelling, the observed out-of-plane energy is well explained by underside reflections off a sharp reflector at the base of the subducted lithosphere. We also detect weaker reflections corresponding to the tomographically mapped top of the slab, which may arise from the boundary between the Nazca plate and the overlying former basaltic oceanic crust. The joint interpretation of the waveform modelling and geodynamic considerations indicate mass flux of the former oceanic lithosphere and basaltic crust across the 660 km discontinuity, linking processes and structure at the top and bottom of the Earth's mantle, supporting the idea of whole mantle convection.

Key words: Mantle processes; Body waves; Wave scattering and diffraction; Subduction zone processes; Dynamics of lithosphere and mantle.

INTRODUCTION

Tomographic inversions for *P*- and *S*-wave seismic velocities in the Earth's mantle suggest that in several places, subducted oceanic lithosphere descends through the mantle transition zone (410–660 km) and penetrates into the lower mantle (e.g. Gu *et al.* 2001; Kárason & van der Hilst 2001; Grand 2002). Suggestions of whole mantle convection have come from these and a variety of studies over several decades (Morgan 1971; Hager *et al.* 1985; van der Hilst *et al.* 1991). In most tomographic models, the seismic velocity perturbation attributed to a subducted slab decreases dramatically or disappears in the mid and lower mantle (Masters *et al.* 2000). The diminished mid-mantle amplitudes could be attributed to slabs warming up below 660 km, reduced tomographic resolution with depth due to large spatial averaging or slabs not penetrating to the deepest mantle, that is, layered mantle convection.

A number of forward modelling studies have found seismic reflections from the lowermost mantle, the D″ layer, and suggested that ancient subducted materials were the cause of these reflections (e.g. Wysession 1996; Scherbaum *et al.* 1997; Wysession *et al.* 1998; Garnero 2000; Thomas *et al.* 2004; Hutko *et al.* 2006). The recent discovery of the post-perovskite phase transition (Murakami *et al.* 2004; Oganov & Ono 2004) has provided a more parsimonious explanation of the seismic reflections (Hernlund *et al.* 2005; van der Hilst *et al.* 2007). Still, deeply penetrating slab material is certainly consistent with geodynamic calculations (e.g. Lithgow-Bertelloni & Richards 1998; Kellogg *et al.* 1999; McNamara & Zhong 2005) and flow inferred from D″ seismic anisotropy studies (Kendall & Silver 1998; Lay *et al.* 1998). The presence of the post-perovskite phase transition may also depend on colder material being subducted into the lowermost mantle (e.g. Hernlund *et al.* 2005).

In some regions, stagnation and ponding of the subducted former oceanic lithosphere in the mantle transition zone above 660 km depth has been noted (Fukao *et al.* 1992), possibly due to the endothermic phase transition of mantle minerals at 660 km depth, which with the expected viscosity increase, can act as a barrier to flow (Tackley *et al.* 1993). Observations of localized seismic wave reflections in the upper part of the lower mantle suggest slabs descending below the 660 km phase boundary (Kaneshima & Helffrich 1998; Kaneshima & Helffrich 1999; Krüger *et al.* 2001). Recently,

*Now at: Department of Geology and Geophysics, Yale University, New Haven, USA.

Cao & Romanowicz (2007) observed *PKPbc* precursors in the depth range from 2270 to 2890 km, indicating that the observed scattered waves can be attributed to the remnants of subducting slabs beneath northwestern North America. They suggest that the subducting slabs could have retained compositional features for many million years. Rost *et al.* (2008) find reflections from sharp reflectors in the Mariana and Tonga regions, down to 1000 km depth from out-of-plane scattered *P* waves. They explain their observations with reflections from the former crust/lithosphere transition in the subducted Mariana and Tonga slabs. These analyses appear to support inferences, drawn from tomographic studies, that slabs subduct well into the lower mantle.

Geodynamic simulations not only show downwellings extending to the deep mantle but emphasise the importance of convective return flow. For example, using plate motions over the last 119 Myr as a surface boundary condition, McNamara & Zhong (2005) show that deep mantle thermochemical structures can be swept into shapes similar to tomographically-observed large-scale low-velocity provinces in the lowermost mantle. This implies that slabs, if subducted to the lowermost mantle, may play a key role in the stirring and organisation of deep mantle heterogeneities. It is important to note that although these ideas are consistent with the fate of slabs within the lowermost mantle, these studies do not mandate it. We require more information about the elastic structure in the lower mantle beneath regions of subduction.

In this study, we investigate the lower mantle beneath the Cocos plate, extending from Central America into the Caribbean. The long-lived subduction for this region (Lithgow-Bertelloni & Richards 1998; Ren *et al.* 2007) may be responsible for the high lower-mantle seismic velocities in tomographic images (Romanowicz 1991; Masters *et al.* 2000; Ritsema & van Heijst 2000; Kárason & van der Hilst 2001; Gu *et al.* 2001; Grand 2002) relating to the Lesser Antilles slab combining with the Farallon/Cocos/Nazca slab under the Caribbean (Ren *et al.* 2007). Many studies have suggested the heterogeneous D″ structures in the lowermost mantle in this region are, at least in part, due to ancient slabs. It is therefore reasonable to expect detection of slabs descending in the mid and lower mantle. In what follows, we employ a newly developed seismic wavefield migration method to search for any scattered energy throughout the lower mantle that may be reflected by descending slabs. Significant scattering is found, which we relate to the rich subduction history in this region.

DATA AND METHOD

We use high-quality broad-band *P*-wave data from 14 intermediate- and deep-focus events in South America (Table 1), recorded at several Californian seismic networks (Fig. 1). The data were normalized to the amplitude of the direct *P*-wave, and a low-pass filter of 1 s was applied to the data to remove high-frequency noise. As a preliminary analysis, we searched for anomalous seismic energy with slowness and backazimuth, distinguishably different from expected seismic arrivals. Seismic recordings were shifted in time, corresponding to a range of slowness and backazimuth combinations and then stacked. We find significant out-of-plane energy in our study region; the slowness–azimuth combinations of the arrivals are similar to previously observed arrivals that were explained as reflections from scatterers (possibly slab material) in the mid mantle (Weber & Wicks 1996; Kaneshima & Helffrich 1998). Fig. 2 shows clear evidence of an out-of-plane arrival. This indicates that energy propagates from the earthquake source to an out-of-plane reflector and onto the seismic recording station with a backazimuth detectably different from the great circle path. In the left-hand panel of Fig. 2, the direct *P*-wave is seen to arrive with the expected azimuth and slowness, 134° ($\mathrm{baz}_{\mathrm{theo}}$) and 5.8 sdeg^{-1}, respectively. In the right-hand panel of the figure, an arrival can be seen with a slowness similar to that of the *P*-wave but with a backazimuth that is ∼10° from the great circle path. In general, we find out-of-plane arrivals from the east of the great circle plane corresponding to the expected direction of the subducted Farallon/Nazca plate. The right-hand panel also shows a second arrival along the great circle arc with a slowness slightly higher than that for the direct *P*-wave. This is the depth phase *pP*, the source-side reflection from the surface that arrives with the expected slowness.

Table 1. Events used in this study.

Event	Date (year-month-day)	Latitude (deg)	Longitude (deg)	Depth (km)
1	1998-OCT-8	−16.12	−71.40	136.0
2	1999-SEP-15	−20.93	−67.28	218.0
3	1999-NOV-21	−21.75	−68.78	101.0
4	2001-JUN-19	−22.74	−67.88	146.0
5	2001-JUN-29	−19.52	−66.25	273.0
6	200-MAR-28	−21.66	−68.33	125.0
7	2003-JUL-27	−20.13	−65.18	345.0
8	2003-SEP-17	−21.47	−68.32	127.0
9	2004-MAR-17	−21.12	−65.59	289.0
10	2004-NOV-12	−26.70	−63.32	568.0
11	2005-MAR-21	−24.98	−63.47	579.0
12	2005-JUL-26	−15.35	−72.96	110.0
13	2005-AUG-14	−19.78	−68.98	113.0
14	2005-NOV-17	−22.32	−67.89	162.0

Note: Source parameters have been taken from the preliminary determinations of epicentres (PDE) catalogue.

We use the newly developed slowness backazimuth weighted migration (SBWM) method (Kito *et al.* 2007a) to perform a systematic search for subtle out-of-plane energy in the teleseismic field. The SBWM method is based on a standard Kirchhoff migration scheme, which additionally incorporates the slowness and backazimuth information of the observed wavefield. To suppress undesirable artefacts which arrive at incorrect slowness and backazimuths, we use deviations in slowness and backazimuth (observed minus theoretical) as a weighting factor, which is then applied to the energy calculated, using the Kirchhoff migration scheme (Kito *et al.* 2007a). Furthermore, we mask out a ±5 s time window around known seismic arrivals (such as *pP*, *sP*, *PcP*, etc.) and −5 to +7 s around the direct *P*-wave. This process permits a robust search for seismic heterogeneities, highlighting the reflection locations associated with migrated energy. An orthorhombic 3-D volume of migration gridpoints from 660 km to the core—mantle boundary (CMB) was defined, with vertical and horizontal grid intervals of 10 and 50 km. A horizontal slice through the volume extends 3050 km × 3050 km. Theoretical traveltime, backazimuth and slowness were computed for each gridpoint to each earthquake and seismic recording site, using the IASP91 reference earth model (Kennett & Engdahl 1991).

Seismograms are time-shifted with respect to the theoretical traveltimes and the squared amplitudes stacked in a 3 s time window around the theoretical arrival, calculated using IASP91. The length of the time window is based on the frequency content in the seismic arrivals. Gaussian functions are calculated at each gridpoint and centred on the theoretical slowness and backazimuth with widths of ±1 sdeg^{-1} in slowness and ±10° for the backazimuth. Weighting factors are defined as the corresponding values of the Gaussian functions

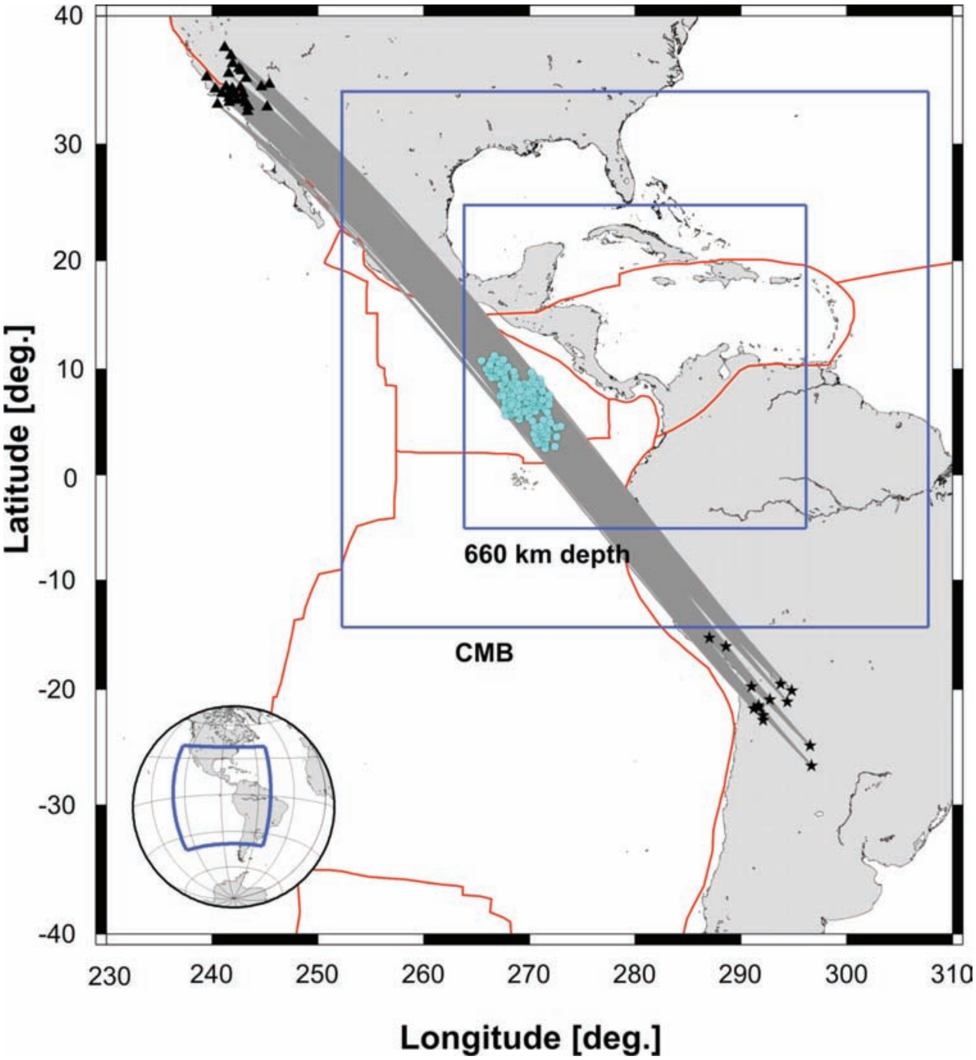

Figure 1. Receivers (triangles) and earthquakes (stars) used in this study. Grey lines indicate great circle paths for each source–receiver combination. Blue circles are *PcP* reflection points. Blue boxes outline the migration volume at the depth of 660 km and the CMB. Red lines indicate plate boundary locations (Gudmundsson & Sambridge 1998).

at the observed slowness and backazimuth (using a 10 s time window). These weighting factors are then applied to the stacked energy. Additionally, the estimated energy using SBWM is stacked event by event to extract the coherent reflected energy from all events (Fig. 3a). Stacking, using all events, helps to suppress spurious energy, potentially generated by structural heterogeneities in the source region. Scattering structures in the great circle path direction are less well constrained than those perpendicular to this direction. Synthetic tests show the resolution of the method is around 50 km, perpendicular to the great circle path. Migrating synthetic data for one event (2004 Nov. 12, 21 stations) with an added reflection from a point (lat. = 13.03°, lon. = −72.81°, depth = 1880 km), we find that the resolution without the slowness and backazimuth weighting is around 20° along the great circle path. Using the SBWM we can improve this resolution to approximately 10° (Kito *et al.* 2007a).

RESULTS

Fig. 3(a) shows seismic energy computed using the SBWM method within our 3-D volume. Strong scattering locations are present to the east of the great circle planes and trend from southeast to northwest (Fig. 3b). This southeast–northwest trend is due to the poor resolution in the direction of the great circle path. Several regions show significant energy in the migration volume. Figs 3(c) and (d) show cross-sections through the 3-D volume parallel and perpendicular to the great circle paths, as indicated by the two lines in Fig. 3(b). Fig. 3(c) highlights several well-resolved reflection areas within the lower mantle. Fig. 4 shows examples of stacked waveforms for two selected gridpoints with large amplitude reflected energy. Coherent seismic energy is visible well above the noise level at backazimuths, which deviate from the great-circle path, and with slowness values distinguishably different from any expected seismic arrivals. The distribution of energy in Fig. 3(c) indicates that the reflections form a continuous band from about 800 km almost to the CMB. In this particular cross-section, we also observe smaller reflections to the east of the continuous band of reflectors. Fig. 3(d) is a cross-section along the great circle path. The resolution along the great-circle path is around 20° without the weighting scheme applied. Despite applying the SBWM method, we find that the migrated images are elongated along the great circle path. Migrating different events

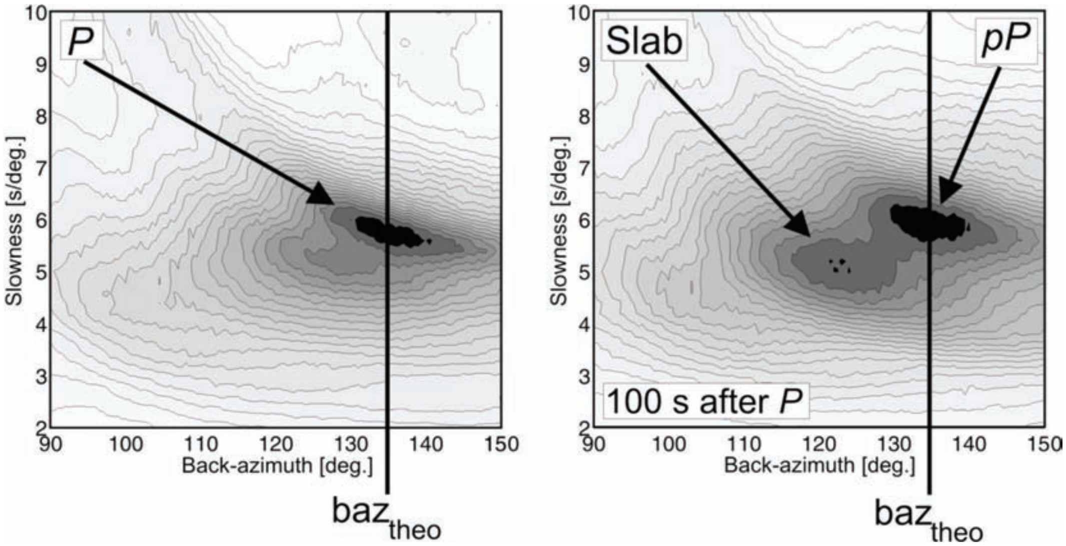

Figure 2. Out-of-plane arrivals estimated by stacking with slowness backazimuth plots (slowness measured in s deg^{-1}, backazimuth, baz, in degrees and amplitude of the stacks contoured in 3 dB lines) for the event 2000 May 12 (South America recorded at the ANZA array in California). The theoretical backazimuth is 134° (baz$_{theo}$); the theoretical slowness is 5.8 s deg^{-1}. In the left-hand side panel, the *P*-wave arrives with the theoretical azimuth and slowness. On the right-hand side panel, an arrival can be seen with a slowness similar to the *P*-wave slowness but a backazimuth about 10° lower than for *P* indicated by 'slab'. A 50 s time window was used for the analysis, which may cause the arrival from other, standard, phases in the same figure, for example, *pP*.

shows similar large amplitude features in the same lower mantle region, and we find the most robust regions of large scattering by stacking all of the events with adjacent regions showing low stacked amplitudes.

We generate synthetic seismograms using the same source–receiver geometry as the data with the reflectivity method (Müller 1985), using the IASP91 1-D reference earth model (Kennett & Engdahl 1991). We migrate the synthetics using the identical procedure to that used with the data. Fig. 5 shows a comparison between the migrated energy calculated from the observed data and that calculated from the synthetics. The observed and synthetic data can be compared directly because the migrated energy in both figures has been normalized by the unmasked *PcP* phase.

Except for anticipated phases, the synthetic migration lacks any out-of-plane energy or artefacts such as *PcP* and underside reflections from the 660 km mantle discontinuity, $P^{660}P$. This confirms the observed out-of-plane reflected energy is not the mis-mapping of known seismic phases introduced by the SBWM method. Seismic energy from events at all source depths map into similar high amplitude reflections shown in Fig. 3; mis-mapping of energy reflected at the Earth's surface is not the source of our observations because energy associated with depth phases would not stack coherently.

Fig. 6 compares locations of the highest amplitude reflections with cross-sections through *P*- and *S*-wave tomographic models. The strongest scatterers are predominantly distributed along the lower edge of the highest velocities in the tomographic slices, but some reflections are also apparent in the D″ region. The geometries of the ray paths, tomographically-imaged subducted slab and the oceanic trench suggest that the strongest reflection locations may delineate the western lower boundary of subducted material from a depth of 800 km down to the D″ layer. Offsets between the reflection points and the edge of the tomographically-imaged high velocity anomalies are observed in certain areas of our cross-sections and are due to the curvature of the subducted slab in this region. The reflection points are generated by a stack of cross-sections of ±2° from the profile whereas the tomographic cross-sections are from a single profile.

Using the waveforms shown in Fig. 4, we investigate reflected wave amplitudes, reflection coefficients and angles of incidence upon both high- and low-velocity lamella, using synthetic waveforms. A simple reflector, that is, a single velocity jump, can not explain the additional swings in the observed waveform. To produce the out-of-plane reflections observed with the SBWM method, in this study, the velocity gradient between the ambient mantle and the slab must be less than 50 km. Assuming a 2 per cent velocity contrast, the low- or high-velocity lamella has to be of the order of 10–15 km to produce the duration and shape of the waveforms shown in Fig. 4. The lamella model is one possible structure that could produce the observed waveform, but other mechanisms can explain the observed seismic reflections and will be discussed in the next section. Reflections from the upper boundary of the slab are less well detected, which may be due to longer wave paths and the attenuation caused by more heterogeneous structures within the slab. Discrete sharp reflectors in the lower mantle have been observed previously (Kaneshima & Helffrich 1999; Krüger *et al.* 2001; Rost *et al.* 2008; Cao & Romanowicz 2007). A continuous band of reflections throughout the entire lower mantle, as shown here, has not been observed before.

DISCUSSION

The seismically observed sharpness (i.e. 10–15 km) of the transition between subducted slab and the surrounding mantle is not expected for a thermal slab that warms up as it subducts. The seismic velocity contrast of the slab–mantle boundary should become increasingly smeared and diffused with depth (Davies 1999; Ricard *et al.* 2005). This would result in reduced amplitudes of the reflectors and a large gradient zone between the mantle and the cold inner part of the slab. A number of phenomena may give rise to a relatively sharp underside slab boundary. Prior to subduction, the depleted harzburgitic oceanic lithosphere of the Nazca plate is predicted to be chemically distinct from the more fertile underlying lherzolitic asthenosphere (Hirth & Kohlstedt 1996), which should give rise to

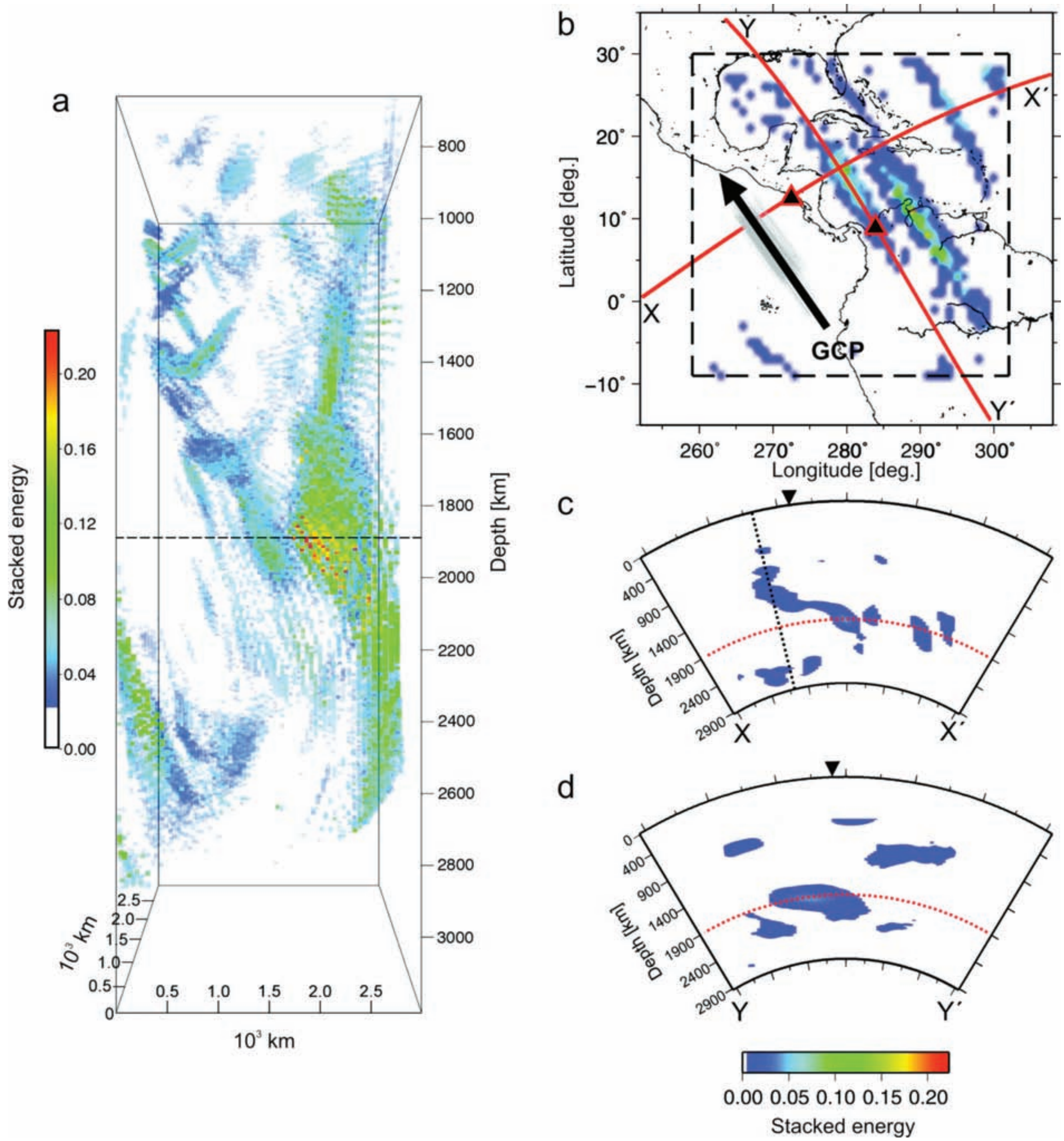

Figure 3. (a) Seismic reflections estimated using the SBWM method within the 3-D volume plotted in a Cartesian coordinate system. The grid spacing is 50 km in the horizontal plane and 10 km in depth throughout the box. The origin of the box (0, 0) is located at −14.37° latitude and 252.26° longitude, at the CMB. The left- and right-hand sides correspond to west and east, respectively, with the view being from the south, facing north. Gridpoints with energy less than 10 per cent of the maximum are omitted. A quadratic opacity function is applied so that lower energies are rendered more transparent. (b) A horizontal cross-section through the 3-D image at a depth of 1880 km, indicated by the dotted black line in (a). The two red lines show the locations of the cross-sections of panels (c) and (d), and the grey lines indicate *PcP* ray paths in the lowermost 100 km of the mantle. The direction of the great circle path is indicated by the black arrow. The dashed line shows the lateral extension of the 3-D grid volume at 1880 km depth. Perpendicular cross-sections (c) and (d) show the depth distribution of the stacked energy. The migrated energy along the five parallel cross-sections centred at the red lines in (b) with 1.0° intervals has been stacked to find robust reflected energy. Subsequently the stacked energy has been divided by 5. Gridpoints with energy less than 2 per cent of the maximum are omitted. The inverted triangles in (c) and (d) correspond to triangles in (b) for better orientation, and the black and red dashed lines correspond to the location of the great circle path and horizontal cross-section at 1880 km respectively.

seismic reflections (Evans *et al.* 2005) and could be the origin of the Gutenberg discontinuity (Gaherty *et al.* 1999; Kumar *et al.* 2007). The elastic contrast associated with this chemical boundary may therefore persist into the lower mantle.

Plume melting beneath the oceanic lithosphere may produce a low-viscosity region of thickness of the order of 15–25 km (Phipps Morgan *et al.* 1995; Phipps Morgan *et al.* 2007), which can be entrained in deep subduction as a thin sheet of former asthenospheric

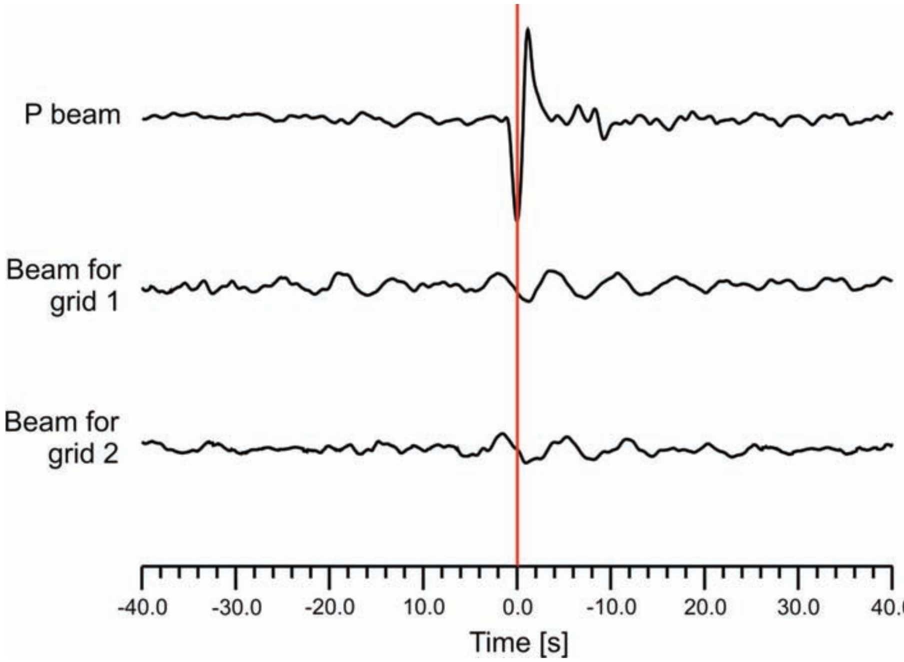

Figure 4. Seismogram sections for the event on 2004 Nov. 12, showing the *P*-wave beam and beams for two out-of-plane gridpoints (gridpoint 1: latitude = 13.035°, longitude = −72.811°, depth = 1880 km and gridpoint 2: latitude = 27.762°, longitude = −61.317°, depth = 1820 km) where large energy is observed.

material beneath the chemically distinct slab (Phipps Morgan *et al.* 2007). This may produce a region of shear between the slab and the underlying mantle, which also could give rise to a sharp reflection. Potentially, a low-viscosity layer of thickness of the order of 10–25 km, with a density or velocity contrast, causes constructive interference from energy reflecting off the top and bottom of the lamella, increasing the apparent duration of the reflected waves. This agrees with observations: many of our observed reflections possess a longer duration than the direct *P*-wave (e.g. Fig. 4). Asthenospheric entrainment and subduction of the former Gutenberg discontinuity explains isolated sharp reflectors from the underside of a slab in the upper mantle, detected beneath Japan (Tonegawa *et al.* 2006).

It has also been shown that lithospheric material subducting into the lower mantle can generate strain beneath downwellings, which has been proposed to generate anisotropy through lattice preferred orientation (McNamara *et al.* 2003). This may imply that a mechanical boundary could be the cause for our reflections, however, this region of anisotropy may be fairly wide (McNamara *et al.* 2003). In contrast, the model of Phipps Morgan *et al.* (2007) mentioned above would produce a thinner layer of anisotropy at the underside of a slab compared with the model of McNamara *et al.* (2003), since the region of shear is contained inside the high-viscosity layer.

Some indications for reflections near the implied upper boundary of the subducted slab (Figs 3 and 6) are present in our migration volume. Weak reflections from the upper boundary of the former oceanic lithosphere could be generated by waves scattering from former mid-ocean ridge basalt (MORB) oceanic crust. Although the detailed structure of descending slabs is not well known, experimental results show that MORB is denser than the average mantle when brought to the pressure and temperature conditions of the lower mantle and will therefore sink into the lowermost mantle (Hirose *et al.* 1999).

We also observe *P*-wave reflections from the top of D″, *PdP*, at approximate depths of 2650 and 2500 km. These correspond to the upper boundary of the high velocities in the lowermost mantle in the tomographic models (Fig. 6). This region has been extensively studied using shear waves (*SdS*), but few *PdP* studies exist (Kito *et al.* 2007b). A discontinuity at the top of D″ has been recently attributed to a phase change in magnesium silicate perovskite to a post-perovskite structure (Murakami *et al.* 2004; Oganov & Ono 2004; Tsuchiya *et al.* 2004; Wookey *et al.* 2005). Although D″ reflections alone do not mandate that D″ is a slab graveyard, they are consistent with the cold, continuous lower mantle slab we image here (Hernlund *et al.* 2005; Hutko *et al.* 2006; Kito *et al.* 2007b). We have observed seismic reflections continuously throughout the lower mantle, which may not be entirely consistent with previous 1-D waveform modelling that suggests that the *S*-wave velocity structure above the D″ is similar to PREM beneath Central America (Ding & Helmberger 1997). *S*-wave studies in this region (e.g. Lay & Helmberger 1983; Kendall & Nangini 1996; Wysession *et al.* 1998) have suggested the top of the D″ is located around 250 to 300 km above the CMB, which is consistent with our *P*-wave observations in this study and with the *P*-wave structures found by Kito *et al.* (2007b).

Fig. 7 shows the set-up of our experiment and the results. It depicts a downgoing slab, underlain by a chemically or mechanically distinct layer and MORB-crust attached to the top. Slab thickening with depth, as indicated by the tomographic models and in our cartoon, may arise from increasing mantle viscosity or slab folding and buckling; the latter has been advocated in both geodynamic (Ribe *et al.* 2007) and seismic (Garnero *et al.* 2007) experiments.

A potential outcome of subducting chemically distinct material to the base of the mantle is that it may succumb to the eventual fate of being swept laterally along the CMB, towards either the Mid-Pacific or Africa, contributing towards the formation and longevity

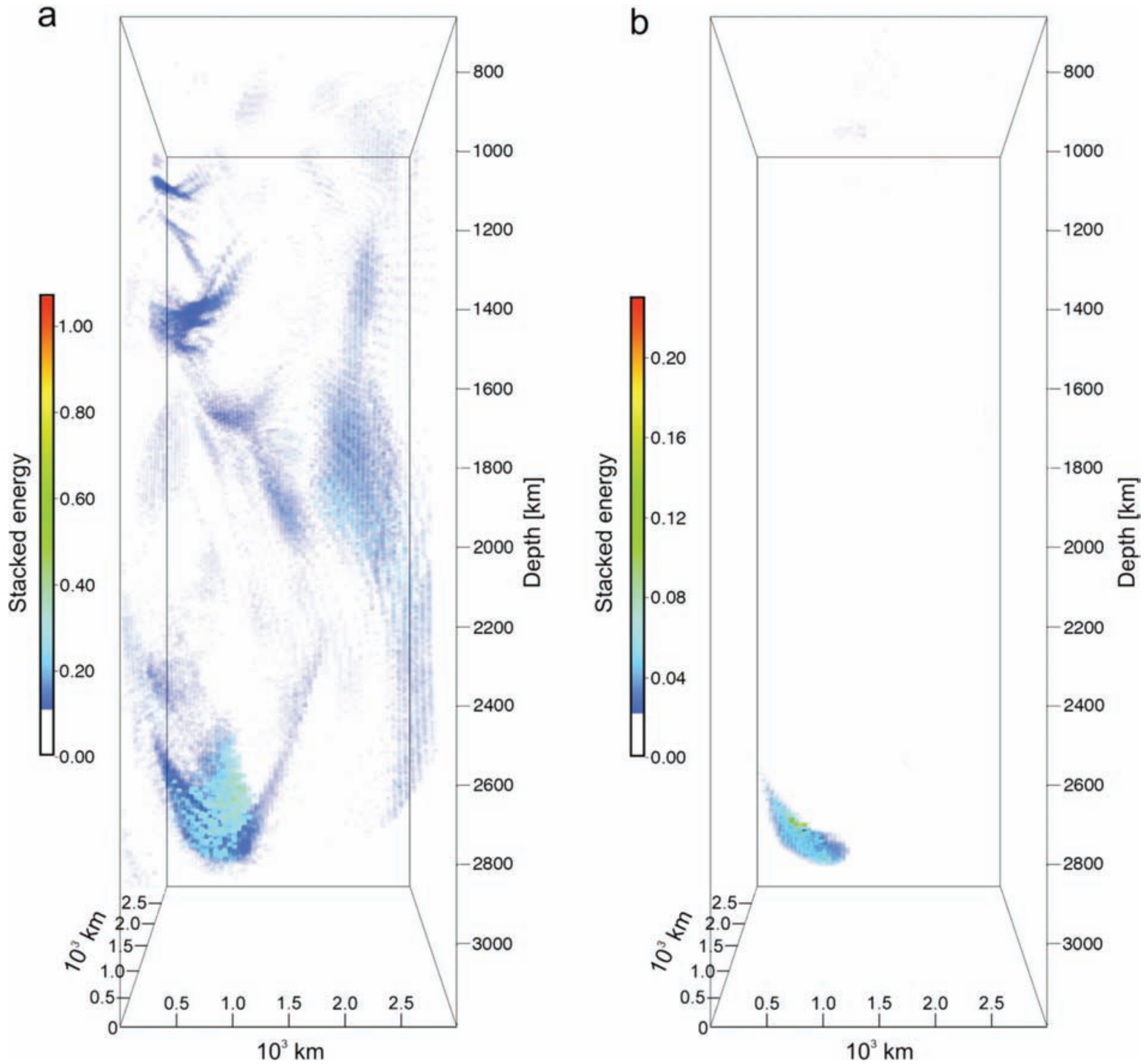

Figure 5. Comparison of migrated observed data with synthetics. The figure for the data (a) is the same as in Fig. 3(a), however, the *PcP* reflection has not been masked to allow a comparison with the synthetic data (b). The synthetic model is IASP91, a 1-D radially symmetric model that should show no out-of-plane reflections. (b) shows the *PcP* reflection which would normally be masked in the migration before stacking. The migrated energy in both figures has been normalized by the *PcP* energy to allow a better comparison. Gridpoints with energy less than 10 per cent of the maximum are omitted.

of large dense thermochemical piles (Garnero *et al.* 2007) situated beneath upwelling return flow. If a chemical reservoir in the form of a ubiquitous layer exists in the lower mantle, as used to explain the geochemical observations (e.g. Kellogg *et al.* 1999; Boyet & Carlson 2006), deep subduction of slabs, as observed here, would displace such a layer down to the CMB. Considering that deep subduction may have been long lived on Earth, it may be more feasible that chemical reservoirs are in scattered pockets or even within large thermochemical piles. Moreover, convective return flow due to slab descent into the deepest mantle is consistent with the hypothesis that some plumes originate at or near the CMB.

CONCLUSIONS

A new seismic wave migration method has been applied to *P*-wave data to search for seismic reflections that may be associated with subduction. Significant out-of-plane seismic energy has been observed throughout the lower mantle, forming a continuous band of reflections from about 800 km to the CMB. The observed seismic reflections mainly originate from the slab underside, but some weaker reflections are visible from the upper boundary of the subducted slab beneath the Caribbean. Although modelling suggests that the observed waveforms could be explained by 10–15 km thick high- or low-velocity lamellae located at the slab-mantle boundary, several other geodynamic scenarios could be considered to be responsible for the seismic reflections. Causes for the sharp reflectors throughout the lower mantle could be a chemically distinct lower slab boundary such as asthenospheric entrainment by subduction or a mechanical boundary, that is, anisotropy in a thin layer. The reflections we relate to a subducted slab in the lower mantle suggest mass flux across the mantle transition zone, at least in this region, and support the idea of the whole mantle convection.

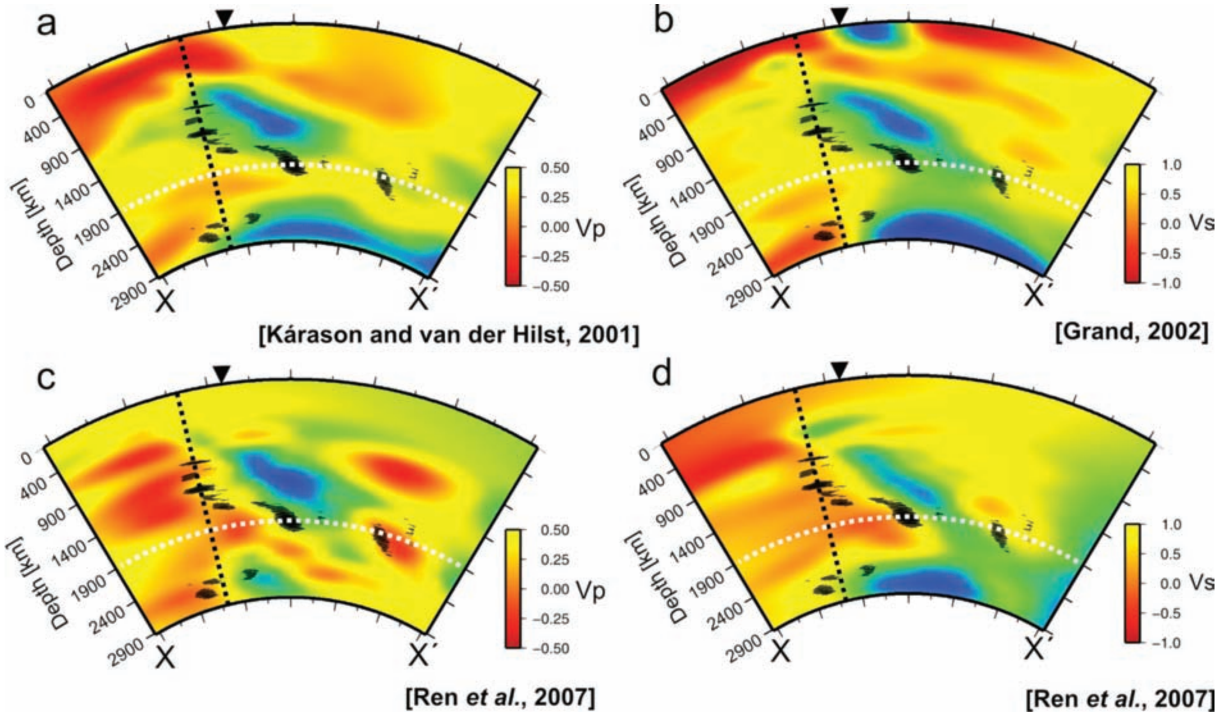

Figure 6. The observed reflection points (black contour lines) are plotted over *P*- and *S*-wave tomographic images (Kárason & van der Hilst 2001; Grand 2002; Ren *et al.* 2007). The tomographic images are based on Kárason & van der Hilst (2001) in (a), Grand (2002) in (b) and Ren *et al.* (2007) in (c) and (d). Five cross-sections (+2° to −2° with 1° spacing interval, from the solid red line perpendicular to the great circle path in Fig. 3b) are stacked and contoured. Gridpoints with energy less than 2 per cent of the maximum are omitted. The subducted lithosphere can be observed as blue/green area in the tomography images. The inverted triangle indicates the west coast of Central America. The white dotted line is the location of the 1880 km horizontal cross-section in Fig 3(b), and the black dotted line indicates the great circle path.

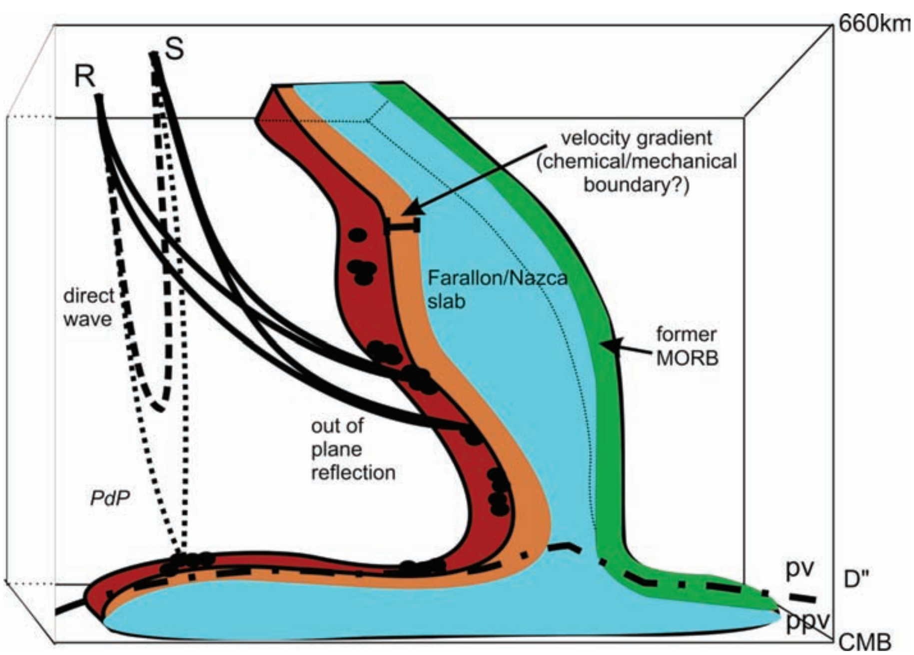

Figure 7. Schematic representation of our experiment geometry. Out-of-plane reflections (solid black lines) are shown together with the direct *P* wave (dashed line) and the reflection from the top of D″, labelled *PdP* (dotted line). R and S indicate 'to receiver' and 'to source', respectively. The slab is shown from the 660 km discontinuity down to the CMB. The black circles indicate areas where we image reflected energy with the SBWM method. The slab is shown with an underside compositional/mechanical boundary (brown), harzburgite (blue) in the middle and former MORB oceanic crust (dark green) at the top side. The distribution of the observed reflections is explained by a sharp reflector at the underside of the slab. The phase transition of perovskite (pv) to post-perovskite (ppv), alternating dashed-dotted line, in the presence of a cold slab is consistent with observed reflections about 300 km above the CMB.

ACKNOWLEDGMENTS

This study is supported by National Environment Research Council (NERC) NE/B000095/1 (TK, CT, AR & AEH) and NE/C000315/1 (SEJN) and a National Science Foundation grant 0135119 (EJG). We thank the IRIS Data Management Center for freely available data. Figures were produced using GMT (Wessel & Smith 1995), and Seismic Handler (Stammler 1993) was used for the data analysis. Fig. 2 has been created, based on M. Wallace's preliminary data analysis. We thank Michael Kendall and two anonymous reviewers for their useful comments which have improved the manuscript.

REFERENCES

Boyet, M. & Carlson, R.W., 2006. A new geochemical model for the Earth's mantle inferred from ^{146}Sm-^{142}Nd systematics, *Earth. planet. Sci. Lett.*, **250,** 254–268.

Cao, A. & Romanowicz, B., 2007. Locating scatterers in the mantle using array analysis of PKP precursors from an earthquake doublet, *Earth. planet. Sci. Lett.*, **255,** 22–31.

Davies, J.H., 1999. Simple analytical model for subduction zone thermal structure, *Geophys. J. Int.*, **139,** 823–828.

Ding, X.M. & Helmberger, D.V., 1997. Modeling D″ structure beneath Central America with broadband seismic data, *Phys. Earth planet. Inter.*, **101,** 245–270.

Evans, R.L., Hirth, G., Baba, K., Forsyth, D., Chave, A. & Mackie, R., 2005. Geophysical controls from the MELT area for compositional controls on oceanic plates, *Nature*, **437,** 249–252.

Fukao, Y., Obayashi, M., Inoue, H. & Nenbai, M., 1992. Subducting slabs stagnant in the mantle transition zone, *J. geophys. Res.*, **97,** 4809–4822.

Gaherty, J.B., Kato, M. & Jordan, T.H., 1999. Seismological structure of the upper mantle: a regional comparison of seismic layering, *Phys. Earth planet. Inter.*, **110,** 21–41.

Garnero, E.J., 2000. Heterogeneity in the lowermost mantle, *Ann. Rev. Earth Planet. Sci.*, **28,** 509–537.

Garnero, E.J., Lay, T. & McNamara, A., 2007. Implications of lower mantle structural heterogeneity for existence and nature of whole mantle plumes, in *The Origin of Melting Anomalies: Plates, Plumes and Planetary Processes*, Vol. **430**, pp. 79–101, eds Foulger, G.R. & Jurdy, D.M., Geological Society of America Special Paper.

Grand, S.P., 2002. Mantle shear-wave tomography and the fate of subducted slabs, *Phil. Trans. R. Soc Lond., A*, **360,** 2475–2491.

Gu, Y., Dziewonski, A., Su, W. & Ekström, G., 2001. Models of the mantle shear velocity and discontinuities in the pattern of lateral heterogeneities, *J. geophys. Res.*, **106,** 11169–11199.

Gudmundsson, O. & Sambridge, M., 1998. A regionalized upper mantle (RUM) seismic model, *J. geophys. Res.*, **103,** 7121–7136.

Hager, B.H., Clayton, R.W., Richards, M.A., Comer, R.P. & Dziewonski, A.M., 1985. Lower mantle heterogeneity, dynamic topography and the geoid, *Nature*, **313,** 541–545.

Hernlund, J.W., Thomas, C. & Tackley, P.J., 2005. A doubling of the post-perovskite phase boundary and the structure of the lowermost mantle, *Nature*, **434,** 882–886.

Hirose, K., Fei, Y., Ma, Y. & Mao, H.K., 1999. The fate of subducted basaltic crust in the Earth's lower mantle, *Nature*, **397,** 53–56.

Hirth, G. & Kohlstedt, D.L., 1996. Water in the oceanic upper mantle: implications for rheology, melt extraction and the evolution of the lithosphere, *Earth planet. Sci. Lett.*, **144,** 93–108.

Hutko, A., Lay, T., Garnero, E.J. & Revenaugh, J.S., 2006. Seismic detection of folded, subducted lithosphere at the core-mantle boundary, *Nature*, **441,** 333–336.

Kaneshima, S. & Helffrich, G., 1998. Detection of the lower mantle scatterers northeast of the Mariana subduction zone using short-period array data, *J. geophys. Res.*, **103,** 4825–4838.

Kaneshima, S. & Helffrich, G., 1999. Dipping low-velocity layer in the mid-lower mantle: evidence for geochemical heterogeneity, *Science*, **283,** 1888–1891.

Kárason, H. & van der Hilst, R.D., 2001. Tomographic imaging of the lowermost mantle with differential times of refracted and diffracted core phases (PKP, Pdiff), *J. geophys. Res.*, **106,** 6569–6587.

Kellogg, L.H., Hager, B.H. & van der Hilst, R.D., 1999. Compositional stratification in the deep mantle, *Science*, **283,** 1881–1884.

Kendall, J.M. & Nangini, C., 1996. Lateral variations in D″ below the Caribbean, *Geophys. Res. Lett.*, **23,** 399–402.

Kendall, J.M. & Silver, P.G., 1998. Investigating causes of D″ anisotropy, in *The Core Mantle Boundary Region*, Vol. 28, Geodynamic Series, pp. 97–118, eds M. Gurnis, M. Wysession, E. Knittle & B.A. Buffett, AGU, Washington DC, USA.

Kennett, B.L.N. & Engdahl, E.R., 1991. Traveltimes for global earthquake location and phase identification, *Geophys. J. Int.*, **105,** 429–465.

Kito, T., Rietbrock, A. & Thomas, C., 2007a. Slowness-Back-azimuth weighted migration: a new array approach to a high-resolution image, *Geophys. J. Int.*, **169,** 1201–1209.

Kito, T., Rost, S., Thomas, C. & Garnero, E.J., 2007b. New insights into the P and S wave velocity structure of the D″ discontinuity beneath the Cocos plate, *Geophys. J. Int.*, **169,** 631–645.

Krüger, F., Baumann, M., Scherbaum, F. & Weber, M., 2001. Mid-mantle scatterers near the Mariana slab detected with a double array method, *Geophys. Res. Lett.*, **28,** 667–670.

Kumar, P., Yuan, X., Kumar, M.R., Kind, R., Li, X. & Chadha, R.K., 2007. The rapid drift of the Indian tectonic plate, *Science*, **449,** 894–897.

Lay, T. & Helmberger, D.V., 1983. A lower mantle S-wave triplication and the shear velocity structure of D″, *Geophys. J. R. astr. Soc.*, **75,** 799–837.

Lay, T., Williams, Q., Garnero, E.J., Kellogg, L. & Wysession, M.E., 1998. Seismic wave anisotropy in the D″ region and its implications, in *The Core Mantle Boundary Region*, Vol. 28, Geodynamic Series, pp. 299–318, eds Gurnis, M., Wysession, M., Knittle, E. & Buffett, B.A., AGU, Washington DC, USA.

Lithgow-Bertelloni, C. & Richards, M.A., 1998. The dynamics of Cenozoic and Mesozoic plate motions, *Rev. Geophys.*, **36,** 27–78.

Masters, G., Laske, G., Bolton, H. & Dziewonski, A.M., 2000. The relative behavior of shear velocity, bulk sound speed, and compressional velocity in the mantle: implications for chemical and thermal structure, in *Earth's Deep Interior: Mineral Physics and Tomography from the Atomic to the Global Scale*, pp. 63–87, eds Karato, S., Forte, A.M., Liebermann, R.C., Masters, G. & Stixrude, L., AGU, Washington, DC.

McNamara, A.K. & Zhong, S., 2005. Thermochmical structures beneath Africa and the Pacific Ocean, *Nature*, **437,** 1136–1139.

McNamara, A.K., van Keken, P.E. & Karato, S., 2003. Lattice-preferred orientation near the core-mantle boundary; a likely mechanism to produce seismic anisotropy, *J. geophys. Res.*, **108**(B5), 2230, doi:10.1029/2002JB001970.

Morgan, W.J., 1971. Convection plumes in the lower mantle, *Nature*, **230,** 42–43.

Müller, G., 1985. The reflectivity method: a tutorial, *J. Geophys.*, **58,** 153–174.

Murakami, M., Hirose, K., Sata, N., Ohishi, Y. & Kawamura, K., 2004. Phase transition of $MgSiO_3$ perovskite in the deep lower mantle, *Science*, **304,** 855–858.

Oganov, A.R. & Ono, S., 2004. Theoretical and experimental evidence for a post-perovskite phase of $MgSiO_3$ in Earth's D″ layer, *Nature*, **430,** 445–448.

Phipps Morgan, J., Morgan, W.J., Zhang, Y.-S. & Smith, W.H.F., 1995. Observational hints for a plume-fed, sub-oceanic asthenosphere and its role in mantle convection, *J. geophys. Res.*, **100,** 12753–12767.

Phipps Morgan, J., Hasenclever, J., Hort, M., Rüpke, L. & Parmentier, E.M., 2007. On subducting slab entrainment of buoyant asthenosphere, *Terra Nova*, **19**(3), 167–173.

Ren, Y., Stutzman, E., van der Hilst, R.D. & Besse, J., 2007. Understanding seismic heterogeneities in the lower mantle beneath the Americas from seismic tomography and plate tectonic history, *J. geophys. Res.*, **112,** B01302, doi:10.1029/2005JB004154.

Ribe, N., Stutzmann, E., Ren, Y. & van der Hilst, R.D., 2007. Buckling instabilities of subducted lithosphere beneath the transition zone, *Earth planet. Sci. Lett.*, **254,** 173–179.

Ricard Y., Mattern, E. & Mattas, J., 2005. Synthetic tomographic images of slabs from mineral physics, in *Earth's Deep Mantle, Structure Composition, and Evolution*, Vol. 160, Geophysical monograph, pp. 283–300, eds van der Hilst, R.D., Bass, J., Mattas, J. & Trampert, J., AGU, Washington DC, USA.

Ritsema, J., & van Heijst, H.J., 2000. Seismic imaging of structural heterogeneity in Earth's mantle: evidence for large-scale mantle flow, *Sci. Prog.*, **83,** 243–259.

Romanowicz, B., 1991. Seismic tomography of the Earth's mantle, *Ann. Rev. Earth planet. Sci.*, **19,** 77–99.

Rost, S., Garnero, E.J. & Williams, Q., 2008. Seismic array detection of subducted oceanic crust in the lower mantle, *J. geophys. Res.*, **113,** B06303, doi:10.1029/2007JB005263.

Scherbaum, F., Krüger, F. & Weber, M., 1997. Double beam imaging: mapping lower mantle heterogeneities using combinations of source and receiver arrays, *J. geophys. Res.*, **102,** 507–522.

Stammler, K., 1993. Seismic handler – programmable multichannel data handler for interactive and automatic processing of seismological analysis, *Computer Geosci.*, **19,** 135–140.

Tackley, P.J., Stevenson, D.J., Glatzmaier, G.A. & Schubert, G., 1993. Effects of an endothermic phase transition at 670 km depth in a spherical model of convection in the Earth's mantle, *Nature*, **361,** 699–704.

Thomas, C., Kendall, J.-M., & Lowman, J., 2004. Lower mantle seismic discontinuities and the thermal morphology of subducted slabs, *Earth planet. Sci. Lett.*, **255,** 105–113.

Tonegawa, T., Hirahara, K., Shibutani, T. & Fujii, N., 2006. Lower slab boundary in the Japan subduction zone, *Earth planet. Sci. Lett.*, **247,** 101–107.

Tsuchiya, T., Tsuchiya, J., Umemoto, K. & Wentzcovitch, R.M., 2004. Phase transition in $MgSiO_3$ perovskite in the earth's lower mantle, *Earth planet. Sci. Lett*., **224,** 241–248.

van der Hilst, R.D., Engdahl, E.R., Spakman, W. & Nolet, G., 1991. Tomographic imaging of subducted lithosphere below northwest Pacific island arcs, *Nature*, **353,** 37–43.

van der Hilst, R.D., de Hoop, M.V., Wang, P., Shim, S.H., Ma, P. & Tenorio, L., 2007. Seismostratigraphy and thermal structure of Earth's core-mantle boundary region, *Science*, **315,** 1813–1817.

Weber, M. & Wicks, C.W., 1996. Reflections from a distance subduction zone, *Geophys. Res. Lett.*, **23,** 1453–1456.

Wessel, P. & Smith, W.H.F., 1995. New version of the Generic Mapping Tools released, *EOS, Trans. Am. geophys. Un.*, **76,** 329.

Wookey, J., Stackhouse, S., Kendall, J.M., Brodholt, J.P. & Price, G.D., 2005. Efficacy of the post-perovskite phase as an explanation of lowermost mantle seismic properties, *Nature*, **438,** 1004–1008.

Wysession, M.E., 1996. Imaging cold rock at the base of the mantle: the sometimes fate of slabs? in *Subduction: Top to Bottom*, Vol. 96, Geophys. Monogr. Series, pp. 369–384. eds Bebout, G.E., Scholl, D.W., Kirby, S.H. & Platt, J.P., AGU, Washington, DC, USA.

Wysession, M.E., Lay, T., Revenaugh, J., Williams, Q., Garnero, E.J., Jeanloz, R. & Kellogg, L.H., 1998. The D$''$ discontinuity and its implications, in *The Core Mantle Boundary Region*, Vol. 28, Geodynamic Series, pp. 273–297, eds Gurnis, M., Wysession, M., Knittle, E. & Buffett, B.A., AGU, Washington DC, USA.